FULL PAPER

Dalton
www.rsc.org/dalton

# Heat capacity of $SrFeO_{3-\delta}$; $\delta = 0.50$, 0.25 and 0.15 – configurational entropy of structural entities in grossly non-stoichiometric oxides †

**Camilla Haavik,[a] Egil Bakken,[a] Truls Norby,[a] Svein Stølen,[a] Tooru Atake[b] and Takeo Tojo[b]**

[a] *Department of Chemistry, University of Oslo, Postbox 1033 Blindern, N0315 Oslo, Norway*

[b] *Tokyo Institute of Technology, Materials and Structures Laboratory, 4259 Nagatsuta-cho, Midori-ku, Yokohama, 226-8503, Japan*

***Received 20th September 2002, Accepted 20th November 2002***
***First published as an Advance Article on the web 24th December 2002***

The heat capacity of $SrFeO_{3-\delta}$; $\delta = 0.50$, 0.25 and 0.15 has been determined for $10 < T/K < \approx 800$ K by adiabatic calorimetry. The total heat capacity has been analysed and the entropy of the magnetic and structural order–disorder transitions derived. The excess heat capacity of $SrFeO_{2.50}$ relative to the mixture of the binary constituent oxides is large even far below $T_N = 685$ K due both to vibrational and magnetic effects. Lattice energy simulations show that the maximum in the excess heat capacity observed at around 60 K is due to a change in the vibrational density of state with origin in changes in the shortest Sr–O bond length on formation of the ternary oxide from the binary ones. While the entropy of the magnetic order–disorder transitions appear to be close to the ideal spin-only values, the entropy of the structural order–disorder transitions are much smaller than expected assuming random distribution of the relevant species on the different sub-lattices. A statistical analysis of the effect of enthalpically preferred structural entities (square pyramids or tetrahedra) on the configurational entropy is presented. A significantly reduced configurational entropy in qualitative agreement with the experiments is obtained.

## Introduction

The energetics of grossly disordered phases is not easily mapped and in particular are energetic contributions of configurational origin difficult to assess. While random distribution-type approximations seem to be appropriate in systems with weakly interacting defects, defects that interact strongly with normal lattice sites and with other defects give a significant degree of short-range order that is often difficult to treat mathematically. When for example a perovskite-type oxide, $ABO_{3-\delta}$, is reduced some of the oxygen atoms are left vacant. A completely random distribution of these vacancies at the oxygen sub-lattice would imply that there is some probability that a B-atom is surrounded by six vacancies. This is extremely unlikely and also energetically unfavorable. This argument is substantiated by the fact that reduced perovskite-type oxides often form ordered structures at low temperatures. In these, the transition metal is coordinated to 6 (octahedral coordination), 5 (square pyramidal coordination) or 4 (tetrahedrally or square planar coordination) oxygen atoms. These structural entities are distributed in a regular way at low temperatures. Fig. 1 shows the ordered arrangement of 50% octahedra and 50% square planar structural entities in $La_2Ni_2O_5$,[1,2] of 50% octahedra and 50% tetrahedra in $Ca_2Fe_2O_5$[3,4] and of 100% square pyramids in $Sr_2Mn_2O_5$.[5] Often only one type of structural entity with coordination number < 6 is observed in a reduced perovskite at low temperatures. Hence, there must be an energetic preference for the observed polyhedrons for a given transition metal in a particular compound. The size of this enthalpic term is not known. In some oxides a mixture of polyhedrons is observed, hence, indicating that the enthalpy difference is not too large. In $La_{8-x}Sr_xCu_8O_{20}$, $CuO_6$ octahedra, $CuO_5$ square pyramids and $CuO_4$ square planar entities are observed.[6] On heating changes in the structures must be expected and phase transitions to disordered modifications are often observed.

The effect of structural entities on the energetics of grossly non-stoichiometric oxides is approached through a study of $SrFeO_{3-\delta}$ ($0 \le \delta \le 0.5$). $SrFeO_{3-\delta}$ is grossly non-stoichiometric at high temperatures. Three reduced, vacancy-ordered low-symmetry phases are formed on cooling.[7] These phases will here be represented by the ideal stoichiometric ratios $SrFeO_{2.875}$ (or $Sr_8Fe_8O_{23}$), $SrFeO_{2.75}$ (or $Sr_4Fe_4O_{11}$), and $SrFeO_{2.50}$ (or $Sr_2Fe_2O_5$). Experimental heat capacities for samples with compositions close to the ideal stoichiometries are reported and the energetics of magnetic and structural order–disorder transitions analysed. Special attention is given to the less than ideal configurational entropy of the structural transitions. This excess entropy has origin in enthalpically favoured structural entities present also in the disordered materials at high temperatures. The thermodynamic properties of $SrFeO_{3-\delta}$ and an analysis of the entropic contribution to the redox energetics have been published earlier.[8]

The phase relations in the $SrFeO_{3-\delta}$ system at low temperatures are complex and not well established. $SrFeO_{2.75}$, $SrFeO_{2.875}$ and $SrFeO_3$ all appear to have homogeneity ranges but the compositional limits can only be vaguely indicated based on literature. Oxygen-rich cubic $SrFeO_{3-\delta}$ seems at room temperature to be stable for $2.92 \le (3-\delta) \le 3.0$.[9] For the phase with ideal composition $SrFeO_{2.875}$, single-phase materials with a similar structure are reported between $SrFeO_{2.83}$[10] and $SrFeO_{2.875}$.[11] A single phase with an orthorhombic superstructure of the basic cubic unit cell has been reported for the composition range from $SrFeO_{2.68}$[7] to $SrFeO_{2.75}$.[10] However, in the course of the present study, small amounts of $SrFeO_{2.50}$ are observed in a sample with the nominal composition $SrFeO_{2.725}$. Hence, the compositional range of the orthorhombic phase seems to be much narrower than earlier proposed. As discussed by Haavik.[12] The ordered low-temperature modification of $SrFeO_{2.50}$, $Sr_2Fe_2O_5$, is close to stoichiometric.[7,13]

$SrFeO_3$ crystallizes in the cubic perovskite structure with all Fe(IV) octahedrally coordinated by oxygen atoms.[11] The stoichiometric compound is antiferromagnetically ordered below $T_N \approx 130$ K.[14] $SrFeO_{2.50}$ is structurally ordered below 1120 K and takes the brownmillerite structure with half of the Fe(III) at octahedrally coordinated sites and half at tetrahedrally

† Electronic supplementary information (ESI) available: the experimental molar heat capacities of $SrFeO_{2.54}$, $SrFeO_{2.725}$ and $SrFeO_{2.833}$ at sub-ambient temperatures and the corresponding data for $SrFeO_{2.50}$, $SrFeO_{2.74}$, $SrFeO_{2.82}$, $SrFeO_{2.833}$ and $SrFeO_{2.85}$ at super-ambient temperatures. See http://www.rsc.org/suppdata/dt/b2/b209236k/

DOI: 10.1039/b209236k

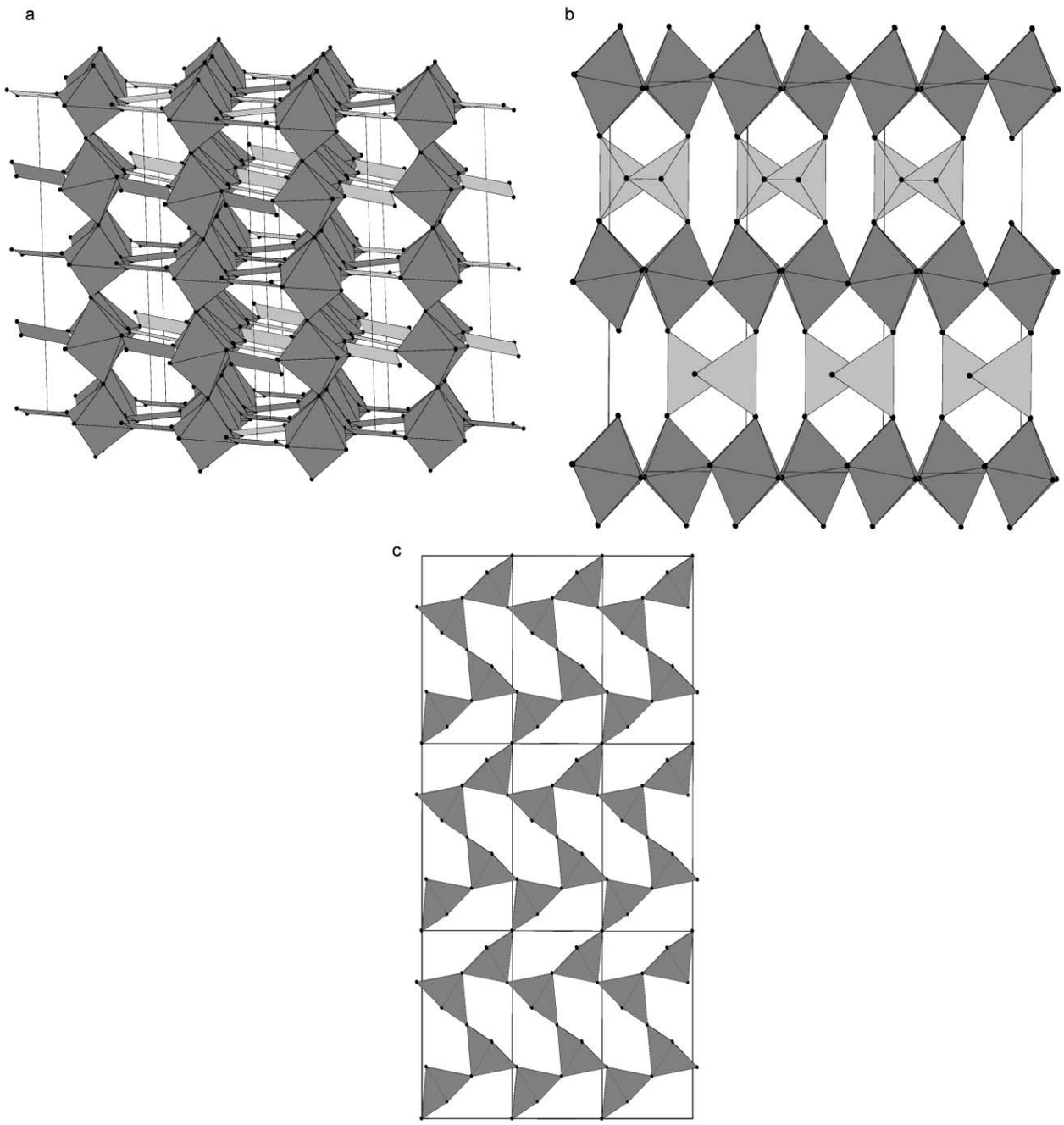


**Fig. 1** Ordered arrangements of the transition metal polyhedra in (a) $La_2Ni_2O_5$ (50% octahedral and 50% square planer entities),[1,2] (b) $Ca_2Fe_2O_5$ (50% octahedral and 50% tetrahedra)[3,4] and (c) $Sr_2Mn_2O_5$ (square pyramids only).[5]

coordinated sites.[7,11,13] $SrFeO_{2.50}$ is an antiferromagnet with Néel temperature reported as 673 [15] or 715 K.[13]

The phase given by the ideal composition $SrFeO_{2.75}$ is reported to be structurally ordered below 670 and 598 K for $SrFeO_{2.75}$ [10] and $SrFeO_{2.73}$,[7] respectively. The low-temperature crystal structure contains two crystallographically distinct Fe-sites: one square-pyramidal, the other octahedral.[11] The distribution of iron-species at the two crystallographic sites is not fully understood. Antiferromagnetic order is observed below 230 K for $SrFeO_{2.76}$.[16] However, only the Fe(III) ions are reported to be magnetically ordered. The Fe(IV) magnetic spins are either in a paramagnetic or in a spin-glass state.[11]

Three distinct Fe-sites in a 1 : 2 : 1 abundance are suggested for the phase with ideal composition $SrFeO_{2.875}$.[11] One site is square-pyramidal (abundance 1) the others are octahedral. $SrFeO_{2.86}$ and $SrFeO_{2.83}$ transform to the disordered high-temperature perovskite-structure at 523 [7] and 570 K.[10] Various Néel temperatures are observed; 80 K has been reported for $SrFeO_{2.84}$,[14] 50 K for $SrFeO_{2.86}$.[17] Additionally, MacChesney *et al.* report several anomalous features in the magnetic properties of $SrFeO_{2.84}$.[14] First of all, the magnetic susceptibility does not obey the Curie–Weiss law at $T_N < T < 200$ K. Second, abrupt changes in the magnetization curve were observed both at 50 and at 63 K. Finally, when $SrFeO_{2.84}$ was cooled in a magnetic field, a remnant magnetization was observed. These features were ascribed to short-range ordering of vacancies on the oxygen sub-lattice.[14]

## Methodology

### Experiments

Sample preparation and characterisation has been reported in detail earlier.[8] Detailed descriptions of the stepwise heated low and high-temperature calorimeters have also been reported. For the low-temperature calorimeter,[18] temperatures were measured

**Table 1** Interatomic potentials parameters for $SrFeO_{2.50}$. The cut-off distance used for the Buckingham potentials is 14 Å

| | Short-range potential representation | |
|---|---|---|
| Interaction | $A$/eV | $\rho$/Å |
| Fe(III) ··· $O^{2-}$ | 3358.400 | 0.2650 |
| $Sr^{2+}$ ··· $O^{2-}$ | 3219.9547 | 0.3067 |
| $O^{2-}$ ··· $O^{2-}$ | 249.3764 | 0.3621 |
| | Shell model parameters | |
| Species | $Y/e$ | $k$/eV Å$^{-2}$ |
| Fe(III) | 1 | 200 |
| $Sr^{2+}$ | 1 | 30 |
| $O^{2-}$ | −2.5 | 27 |

with a platinum resistance thermometer calibrated at the National Physical Laboratory, Teddington, UK, on the basis of ITS-90. The reproducibility of the heat capacity determinations is approximately ±0.05% for 100 < ($T$/K) < 300 and decreases with decreasing temperature to ≈ ±0.20% at 13 K. Sample masses of about 20 g were used in the experiments.

For the high-temperature calorimeter[19,20] samples of masses of 36–59 g were contained in evacuated and sealed vitreous silica containers during measurement. The temperature was measured with an ASL F-18 resistance bridge using locally constructed 25 Ω platinum resistance thermometers. Temperature calibration is performed according to the recommendation of ITS-90 to 933.473 K. The accuracy in temperature determination is considered to be within ± 0.02 K to 903 K, and within ± 0.10 K above 903 K.[20] The accuracy and precision of the heat capacity determinations are approximately ± 0.2%.[20] In the present case relatively low sample masses were used in the calorimetric experiments and the accuracy is probably somewhat lower and estimated to 0.4%.

The enthalpy of the order–disorder transition in $SrFeO_{2.50}$ was determined by differential thermal analysis (Perkin-Elmer DTA 7). The sample, typically around 40 mg, was enclosed in an evacuated and sealed silica tube. An empty evacuated and sealed silica tube was used as a reference. The sample was heated at 10 K min$^{-1}$ and the enthalpy of fusion of Zn, Al, Ag and Au were used for calibration.[21]

### Simulations

Simulations of the heat capacity difference between $SrFeO_{2.50}$ and the binary constituent oxides, SrO and ½ $Fe_2O_3$, are based on an ionic model using two-body potentials to represent short-range forces whereas the Ewald summation is used for the long-range Coloumbic interactions.[22] A conventional Born-model was used, assigning integral ionic charges, based on accepted chemical valence rules, to all species (*i.e.* 2+ to Sr, 3+ to Fe and 2− to O). Cation–oxygen interactions were described by a set of 2-body inter-ionic Buckingham potentials, of the form:

$$\varphi(r) = A\exp\left(-\frac{r}{\rho}\right)$$

where the constants $A$ and $\rho$ are listed in Table 1 and $r$ is the inter-ionic distance. Account of the oxide ion polarisability was taken using the shell model of Dick and Overhauser.[23] The shell charge and spring constants used are also given in Table 1. This set of potentials was developed to reproduce closely the lattice parameters and average Fe–O bond lengths of the ordered low-temperature orthorhombic form of $SrFeO_{2.5}$ as shown in Table 2 where we compare experimental and simulated structural data.

## Results and discussion

### Heat capacity and transition temperatures

The experimental molar heat capacities of $SrFeO_{2.54}$, $SrFeO_{2.725}$ and $SrFeO_{2.833}$ at sub-ambient temperatures and the corresponding data for $SrFeO_{2.50}$, $SrFeO_{2.74}$, $SrFeO_{2.82}$, $SrFeO_{2.833}$ and $SrFeO_{2.85}$ at super-ambient temperatures are given as ESI.

$SrFeO_{2.5}$ is magnetically ordered below $T_N \approx 700$ K[13,15] and the broad heat capacity shoulder with maximum at around 685 K reflects the order–disorder transition. $SrFeO_{2.75}$ is reported to disorder magnetically at $T_N \approx 220$ K[16] and a heat capacity bump is observed in the same temperature region for the $SrFeO_{2.725}$ sample. At 660 K (extrapolated onset) the high-temperature perovskite-phase is formed in agreement with earlier reports; 670 K for $SrFeO_{2.75}$[10] and 660 K for $SrFeO_{2.74}$.[24] The transition temperature reported by Takeda *et al.*,[7] 598 K for $SrFeO_{2.73}$, is significantly lower. Two quite different Néel temperatures are reported for $SrFeO_{2.875}$: 80 K for $SrFeO_{2.84}$[14] and 50 K for $SrFeO_{2.86}$.[17] MacChesney *et al.*[14] report additional anomalous features in the magnetic properties of $SrFeO_{2.84}$ for $T$ < 200 K. The broad heat capacity effect presently observed from 50 to 120 K for $SrFeO_{2.833}$ is thus consistent with MacChesney *et al.*[14] The formation of the high-temperature perovskite phase at around 560 K (extrapolated onset) for samples in the compositional range $SrFeO_{2.82}$ to $SrFeO_{2.85}$ is also in agreement with previous reports, 523 [7] and 570 K.[10]

### Energetics of the magnetic order–disorder transitions

The magnetic order–disorder transition in $SrFeO_{2.50}$ takes place over an extended temperature range, see Fig. 2 and an evaluation of the excess magnetic heat capacity is difficult. The heat capacity at constant pressure can be deconvoluted into contributions of vibrational and magnetic origin (the electronic heat capacity coefficient $\gamma$ is zero for this semi-conductor). The vibrational heat capacity is estimated as the sum of a constant volume heat capacity, $C_V$ and a dilatational contribution, $C_d = \alpha^2 VT/\kappa$, that takes anharmonicity into account. Here $V$ and $\alpha$ are the molar volume and the isobaric (thermal) expansivity, respectively,[7,25–27] while $\kappa$ is the isothermal compressibility.[28] The heat capacity at constant volume, $C_v$, is in the absence of more detailed information on the lattice dynamics of the compound expressed by a single Debye function with a constant $\Theta_D$-value (*i.e.* fixed volume $C_V$). $\Theta_D = 562$ K is estimated from the observed $C_p$ in the region 20–200 K after subtraction of the dilatational contribution. The dashed line in Fig. 2 gives the estimated non-magnetic heat capacity of $SrFeO_{2.50}$. The magnetic entropy above 200 K thus obtained, 4.5 J K$^{-1}$ mol$^{-1}$, is much lower than the magnetic entropy increment expected for

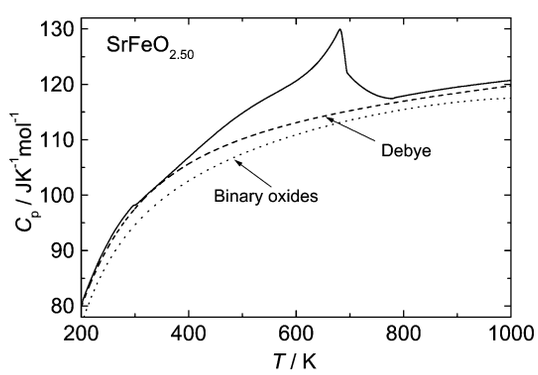


**Fig. 2** The magnetic order–disorder transition in $SrFeO_{2.50}$. The solid line is the presently determined heat capacity. The dashed and dotted lines represent the non-magnetic heat capacity of $SrFeO_{2.50}$, represented by the Debye model and as the sum of heat capacities of the two binary oxides, respectively.

**Table 2** Calculated and experimental[11] unit-cell dimensions and average Fe–O bond lengths for $SrFeO_{2.50}$ (space group *Ibm2*)

| $SrFeO_{2.50}$ | Observed | Calculated | Deviation (%) |
|---|---|---|---|
| *a*/Å | 5.661 | 5.740 | 1.4 |
| *b*/Å | 15.598 | 15.232 | −2.4 |
| *c*/Å | 5.531 | 5.590 | 1.1 |
| *V*/Å$^3$ | 488.39 | 488.69 | 0.1 |
| | Fe(1) site (octahedral) | | |
| Average Fe–O bond length/Å | 2.041 | 2.049 | 0.4 |
| | Fe(2) site (tetrahedral) | | |
| Average Fe–O bond length/Å | 1.909 | 1.874 | −1.8 |

the randomization of the unpaired spins of Fe(III) in the spin-only approximation $R\ln(2S + 1) = 14.9$ J K$^{-1}$ mol$^{-1}$. Since the entropy of the spin transitions in iron oxides generally is in good agreement with ideal spin-only values,[29] the non-transitional heat capacity used in the approximation above may be questioned. Generally the heat capacity of a ternary oxide is well represented by the sum of the heat capacities of the binary constituent oxides. The heat capacity of $SrFeO_{2.50}$ may thus be estimated by using the heat capacities of SrO[30] and ½ α-$Fe_2O_3$ (non-magnetic),[31] see the dotted line in Fig. 2. With this non-transitional heat capacity the magnetic entropy is 8.2 J K$^{-1}$ mol$^{-1}$ for $T > 200$ K. The excess heat capacity of $SrFeO_{2.50}$ relative to the mixture of the binary oxides is plotted together with the analogue excess heat capacities of α-$Fe_2O_3$ [31] and $LaFeO_3$ [32] in Fig. 3.

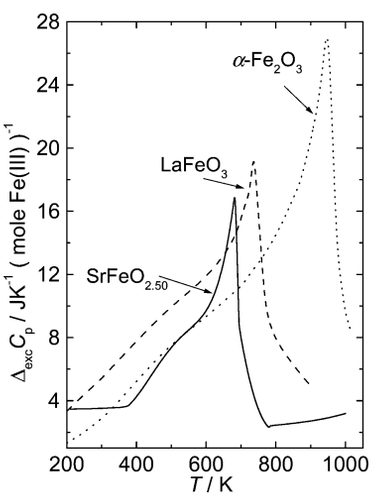


**Fig. 3** The excess heat capacity of $SrFeO_{2.50}$ relative to the mixture of the binary oxides (solid line) compared to the analogue excess heat capacity of $LaFeO_3$[32] (dashed line). The dotted line represents the excess heat capacity of α-$Fe_2O_3$.[31]

The magnetic entropies of $SrFeO_{2.50}$ obtained using the two different estimation schemes are quite different and both are low compared to the theoretical spin-only value. This suggests significant short-range order above the Néel temperature or spin disordering below 200 K. The Debye background is, hence, questionable. Disordering of the spin orientation below 200 K was initially assumed to be negligible. The entropy of $SrFeO_{2.50}$ at 200 K is however 6.7 J K$^{-1}$ mol$^{-1}$ larger than that of a mixture of SrO and (½) α-$Fe_2O_3$. The excess heat capacity of $SrFeO_{2.50}$ relative to the mixture of the binary oxides at $T <$ 200 K is shown in Fig. 4. Two features are obvious: the excess heat capacity is large at 200 K and a heat capacity maximum is observed at around 60 K. The maximum is due to crystal structure effects. Strontium is six-coordinated in SrO and eight-coordinated in $SrFeO_{2.50}$. The increase in coordination number on compound formation leads to longer Sr–O bond lengths and a shift in the vibrational density of state to lower frequencies. Lattice energy simulations qualitatively reproduce this effect. A peak at 100 K corresponds to a difference in the

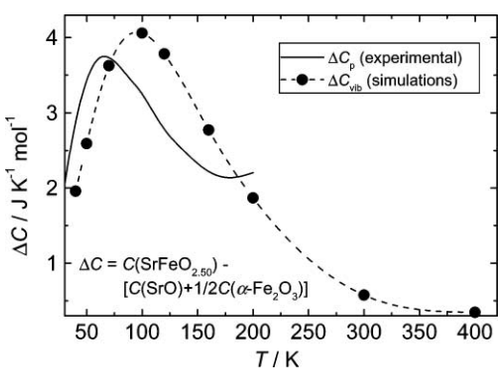


**Fig. 4** The excess heat capacity of $SrFeO_{2.50}$ relative to SrO + (½) α-$Fe_2O_3$, as observed experimentally (---) and as obtained in the simulations (--●--). The dashed line serves as a guide to the eye.

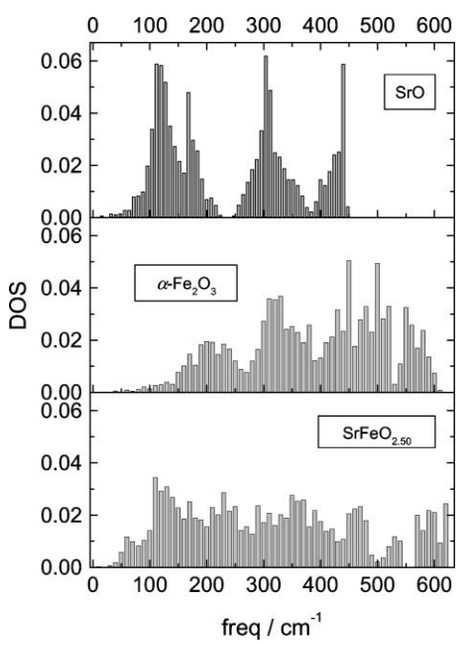


**Fig. 5** Calculated phonon density of states (DOS) for $SrFeO_{2.50}$, SrO and α-$Fe_2O_3$. Note the high DOS of $SrFeO_{2.50}$ at frequencies below 100 cm$^{-1}$.

phonon density of state at low frequencies. The calculated density of states for the three oxides, Fig. 5, shows that the DOS in this region indeed is high in $SrFeO_{2.50}$ compared to a mixture of SrO + (½) α-$Fe_2O_3$. A rough deconvolution of the excess heat capacity of $SrFeO_{2.50}$ at $T < 200$ K, results in a magnetic contribution of approximately 2.5 J K$^{-1}$ mol$^{-1}$ that combined with the contribution at $T > 200$ K gives $\Delta_{magn}S \approx 11$ J K$^{-1}$ mol$^{-1}$.

The disordering of the antiferromagnetically ordered compounds $SrFeO_{2.725}$ and $SrFeO_{2.833}$ is also reflected in the heat capacity, but the transitions are not well defined and take place over large temperature ranges. The effect is easily seen when $C_p/T$ is plotted *versus* $T$. $SrFeO_{2.50}$ serves as a

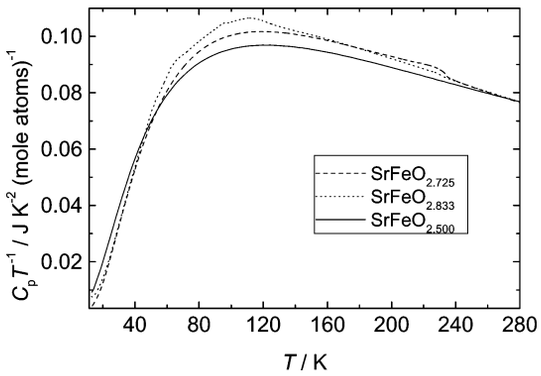


**Fig. 6** Molar heat capacities of $SrFeO_{2.725}$ (dashed line) and $SrFeO_{2.833}$ (dotted line) plotted as $C_p/T$ *versus* $T$ in the temperature range of the magnetic disordering transitions. The curve for $SrFeO_{2.50}$ (solid line) may serve as background.

background in Fig. 6. A first estimate of the magnetic entropy of $SrFeO_{2.725}$ and $SrFeO_{2.833}$ obtained as

$$\Delta_{magn}S = \Delta_0^{300}S\left(SrFeO_{3-\delta}\right) - \frac{(5-\delta)}{4.5}\left[\Delta_0^{300}S\left(SrO\right) + \frac{1}{2}\Delta_0^{300}S\left(\alpha\text{-}Fe_2O_3\right)\right]$$

is 16.0 and 18.3 J K$^{-1}$ mol$^{-1}$. A vibrational entropy contribution due to changes in the local structural environment of Sr when going from the binary to the ternary oxides should be subtracted and the derived magnetic entropies are thus in reasonable agreement with the spin only entropies ($\Delta_{spin\text{-}only}S$ = 14.2 J K$^{-1}$ mol$^{-1}$ for $SrFeO_{2.725}$ and $\Delta_{spin\text{-}only}S$ = 13.9 J K$^{-1}$ mol$^{-1}$ for $SrFeO_{2.833}$).

Neutron-diffraction[24] and Mössbauer[16,33] studies of $SrFeO_{2.75}$ indicate that Fe(IV) is magnetically disordered at low temperatures (4 K). If so the spin-only magnetic disordering entropy (Fe(III) only) is 8.2 J K$^{-1}$ mol$^{-1}$ for $SrFeO_{2.725}$. The presently observed magnetic entropy is larger and suggests that although long-range magnetic order of Fe(IV) is not observed, considerable magnetic short/medium range order is present. The proposed spin-glass structure of the Fe(IV) at low temperature[11] supports this view. The total entropy of $SrFeO_{3-\delta}$ varies, when the structural configurational contribution is subtracted, linearly with composition at high temperatures *e.g.* 1000 K.[8] Adding a theoretical spin-only entropy for Fe(IV) (6.0 J K$^{-1}$ mol$^{-1}$) would lead to an unexpected maximum in entropy *versus* composition.

### Energetics of the structural order–disorder transitions

Only one determination of the enthalpy of the structural order–disorder transition was made for $SrFeO_{2.740}$ and $SrFeO_{2.833}$, giving $\Delta_{struct}H_m$ = 5328 and 2071 J mol$^{-1}$ and, hence, $\Delta_{struct}S_m$ = 7.76 and 3.67 J K$^{-1}$ mol$^{-1}$. For $SrFeO_{2.500}$ the enthalpy and entropy of transition was determined by differential thermal analysis, DTA. The result of four determinations are $T_{struct}$ = 1120 ± 5 K, $\Delta_{struct}H_m$ = 8.5 ± 1.2 kJ mol$^{-1}$, and $\Delta_{struct}S_m$ = 7.6 ± 1.2 J K$^{-1}$ mol$^{-1}$. The estimated uncertainty is twice the standard deviation. The transition temperature and enthalpy of transition compare well with earlier determined values; 1103 [7] and 1123 K [26] for the transition temperature and 7.5 kJ mol$^{-1}$ for enthalpy of transition.[11]

The entropies of transition have three main contributions. The first is the difference in vibrational entropy between the ordered low-temperature phase and the disordered high-temperature phase. The second is the difference in electronic entropy, while the last is the configurational entropy. As a first approximation we will assume that the changes in vibrational and electronic entropy on disordering is negligible. We will also assume that the low temperature structures are completely ordered. Still, the homogeneity regions of $SrFeO_{2.75}$ and $SrFeO_{2.875}$ show that this is a first approximation only (at least for these compositions).

The experimental configurational entropies may be compared with simple estimates assuming random distribution of the different species at the different sub-lattices *i.e.* random distribution of Fe(III) and Fe(IV) on the iron sub-lattice plus random distribution of oxygen ions and oxygen vacancies on the oxygen sub-lattice, see Fig. 7. The experimental configurational entropies are much lower. For $SrFeO_{2.50}$ the difference between the theoretical and experimental configurational entropy certainly is due to short-range order on the oxygen sub-lattice of the disorder phase. The present finding concurs with earlier Mössbauer studies that indicated that the local environment is conserved for many of the iron atoms in the disordered phase.[34] Grenier and co-workers report a gradual change in the oxygen-ion conductivity at $T_{struct}$ and similarly uses this as an argument for the presence of considerable short-range order in the disordered phase.[26]

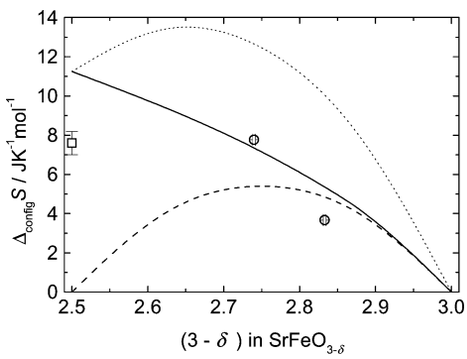


**Fig. 7** Comparison of the ideal configurational entropy, obtained assuming random distribution of the relevant species on the different sublattices, with the experimental configurational entropies for $SrFeO_{2.500}$, $SrFeO_{2.740}$ and $SrFeO_{2.833}$. The solid line gives the configurational entropy corresponding to a random distribution of oxygen atoms and oxygen vacancies on the oxygen sub-lattice. The dashed line results from a random distribution of Fe(III) and Fe(IV) on the iron sub-lattice. The dotted line is the sum of the two contributions.

Also for $SrFeO_{2.725}$ and $SrFeO_{2.833}$ the low configurational entropies may be due to short-range order on the oxygen sub-lattice. In the Mössbauer spectra of the two compositions, a single peak characteristic of a time averaged cubic symmetry was observed at temperatures well above the transition temperature. The transformation to a singlet spectrum however occured gradually with increasing temperature, not suddenly at the transition temperature.[34]

The assumption of random distributions on the different sub-lattices overestimate the configurational entropy and better models are needed. Defect clustering is one, often proposed, solution to the problem. By using the Kröger–Vink approach [35] for $ABO_{3-\delta}$ and by assuming that two effectively negatively charged B-atoms cluster with one effectively positive oxygen vacancy, $V_O^{\cdot\cdot}$, we obtain the following defect reaction

$$2O_O^x + 4B_B^x = 2\langle B_B^{'}\text{–}V_O^{\cdot\cdot}\text{–}B_B^{'}\rangle + O_{2(g)} \qquad (1)$$

where $O_O^x$ is an effectively neutral oxygen atom.

This cluster has been proposed *e.g.* for $LaMnO_{3-\delta}$ by Roosmalen *et al.*[36] If these defect clusters are randomly distributed in the structure the number of possible configurations will be reduced since one cluster will sterically hinder other cluster positions. Hence, defect cluster equations like that given in eqn. (1) may be used at infinite dilution but is inherently incorrect at high defect concentrations if sterical hindrance is not taken explicitly into account (*e.g.* by using a site exclusion factor). An alternative approach that gives under- and over-estimates of the configurational entropy is described below.

**Configurational entropy of structural entities in grossly non-stoichiometric oxides**

Consider a simple non-stoichiometric perovskite-type oxide, $ABO_{3-\delta}$, (A = Ln or Ae and B = a transition metal) with oxygen vacancies and valence defects on the B-sublattice as the only defects. We will assume that A is a cation like $Sr^{2+}$ or $La^{3+}$, which is not involved in the redox reactions, whereas B is present in two oxidation states, $B^{3+}$ and $B^{4+}$ or $B^{2+}$ and $B^{3+}$. Using the former case, all the B-atoms are tetravalent for $\delta = 0$ (*i.e.* in $ABO_3$) and trivalent for $\delta = 0.5$ (*i.e.* in $ABO_{2.5}$). The present contribution is concerned with the configurational entropy due to structural disorder only. Hence, the entropy contribution stemming from electronic defects is not considered presently.

A basic problem in modelling the configurational entropy of a structure based on building blocks that shares corners, edges or faces is that some or all of the atoms belong to more than one basic structural entity. Exact mathematical solutions that describe the distribution of different structural entities in such compounds are not available. In the present treatment estimates of the entropy of compounds containing structural entities are based on what we will call the independent cell approach. Here a given structure is reconstructed into an assemblage of independent cells.

In order to show how the approach works we will first evaluate the entropy of a system were $\delta$ oxygen vacancies and $(3-\delta)$ oxygen atoms are randomly distributed at the oxygen lattice sites in $ABO_{3-\delta}$. The structure is divided into cells consisting of B-atoms surrounded by six-oxygen atoms octahedrally. All possible octahedra are not counted as cells. The cells chosen should (a) be independent *i.e.* not share atoms with other cells and (b) include all oxygen lattice sites in the structure without counting them twice. The structure is reconstructed to consist of ab-stacked "two-dimensional" sheets of cells, see Fig. 8. In

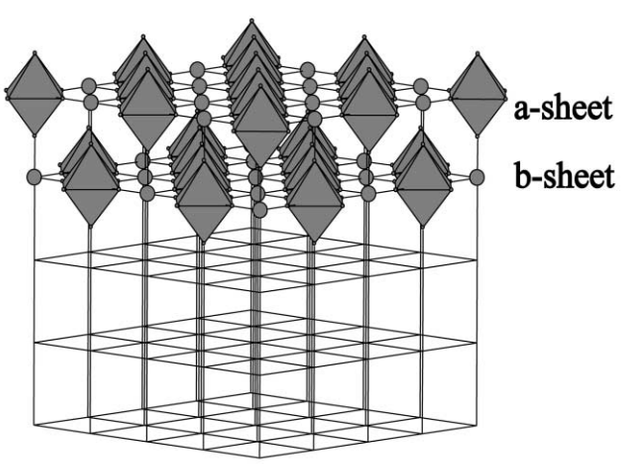


**Fig. 8** Schematic illustration of the independent-cell approach. The structure is reconstructed into ab-stacked "two-dimensional" sheets of octahedra. In the a-sheet every second B-atom form basis for a $BO_6$-cell. The $BO_6$-cells in the b-sheet are shifted one B-atom position with respect to the B-cells in the a-sheet. Thus, all oxygen sites are counted through the defined independent cells. However, only half of the octahedra are counted as cells. The $BO_6$-octahedra that are counted as cells are shown explicitly. The large circles represent B-atoms, which are coordinated by oxygen atoms that are accounted for by the independent cells.

the a-sheet every second B-atom forms the basis for a $BO_6$-cell. The $BO_6$-cells in the b-sheet are shifted one B-atom position with respect to the B-cells in the a-sheet. Thus, all oxygen sites are counted through the defined independent cells. However, only half of the octahedra are counted as cells. The cells can now be treated statistically.

The probability for finding a vacancy at an oxygen lattice site, $P_{V_O}$, in $SrFeO_{3-\delta}$ is

$$P_{V_O} = \frac{N_{V_O}}{3N} = \frac{\delta}{3} \tag{2}$$

where $N_{V_O}$ and $3N$ are the number of oxygen vacancies and the number of oxygen lattice sites. The probability for finding a given number (0 to 6) of vacancies in a given cell is

$$p_j = \lambda_j (P_{V_O})^j (1 - P_{V_O})^{6-j} \tag{3}$$

where $j$ is the number of vacancies in the cell and

$$\lambda_j = \frac{6!}{j!(6-j)!} \tag{4}$$

is the total number of arrangements for a given $j$. The number of ways to distribute the different cells on the total number of cell-sites, $w_{cell}$, is

$$w_{cell} = \frac{(\frac{3N}{6})!}{\prod_{j=0}^{6}(p_j \frac{3N}{6})!} \tag{5}$$

The total number of configurations, $w_{tot}$, can now be found by taking the number of configurations for each cell with $j$ vacancies into consideration

$$w_{tot} = w_{cell} \prod_{j=0}^{6} \lambda_j^{p_j \frac{3N}{6}} = \frac{3N!}{N_{V_O}!(3N - N_{V_O})!} \tag{6}$$

The derived expression is identical to that obtained by using a simple factorial expression and the entropy for a random distribution of oxygen atoms and oxygen vacancies at the oxygen lattice sites is obtained.

For the estimates of the configurational entropy for systems containing structural entities (square pyramids or tetrahedral/square planar entities), larger two-dimensional cells like the (2 × 2), and the (2 × 3) cells of independent octahedra shown in Fig. 9 are constructed. For a specific cell we may allow *e.g.* only

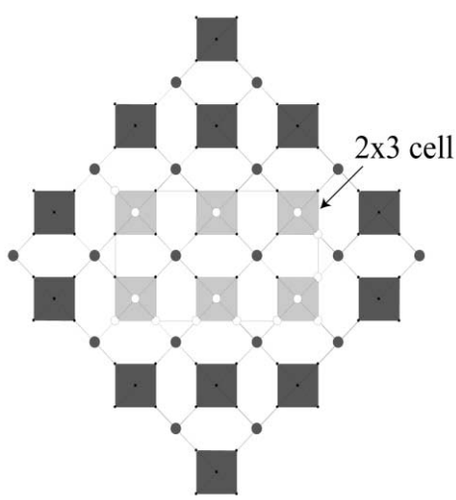


**Fig. 9** Schematic illustration of the (2 × 3) cell. The six independent light grey octahedra belong to a cell. The whole structure is represented by ab-stacking of sheets containing these (2 × 3) cells only. When the defect situation is restricted to square pyramids only, vacancies are not allowed at the oxygen positions represented by open circles. The open circles are located at parts of the equatorial oxygens and at all the apical oxygens of the light grey octahedra. The large black circles represent B-atoms, which are coordinated by oxygen atoms that are accounted for by other cells. Each independent octahedron in a cell is regarded as a polyhedron (octahedron or square pyramid) site.

one vacancy per octahedron and then evaluate the number of configurations manually. If we allow vacancies at the "surface" of the cell the octahedra situated between cells may not obey our restriction of only one vacancy per octahedron. If we on the other hand exclude some of these surface atoms, *i.e.* those given as open circles for the special case of a (2 × 3) cell and assuming only one vacancy per octahedra only, as illustrated in Fig. 9, the restriction is not violated. However, the number of possible configurations for a given cell is then underestimated. Thus two estimates are made; those in which the atoms at the "surface" of the cell either are fully or only partly included. These estimates correspond to overestimates and underestimates, respectively, of the number of possible configurations and thus of the configurational entropy.

The size of the cell is termed $a$ and is 4 for the (2 × 2) cell and 6 for the (2 × 3) cell. Hence, $a$ equals the number of independent octahedra in the cell. Two different defect situations are considered. In the first case square pyramids only are formed on reduction, in the second case tetrahedra are formed as far as possible. Still, one isolated tetrahedron implicitly yields two square pyramids.

For a given cell there is a probability, $P_e$, for finding a certain type of entity in one of the independent polyhedra of the cell. Thus, the probability for finding $j$ entities of a given type is

$$P_j = \lambda_j (P_e)^j (1 - P_e)^{a-j} \quad (7)$$

where

$$\lambda_j = \frac{\alpha!}{j!(\alpha - j)!} \quad (8)$$

is the number of arrangements of $j$ entities of a given type at $a$ independent polyhedron sites in the cell. $\lambda_j$ does not take into account the different orientations each entity may have. An additional term takes this into account; $\varepsilon_j$ includes all configurations of $j$ entities on the polyhedron-sites in the cell for the assumed defect situation. The total number of configurations is then

$$w_{tot} = \frac{(\frac{N}{2\alpha})!}{\prod_{j=0}^{\alpha}(p_j \frac{N}{2\alpha})!} \prod_{j=0}^{\alpha} \varepsilon_j^{p_j \frac{N}{2\alpha}} \quad (9)$$

The number of configurations of $j$ entities of a certain type in the cell, $\varepsilon_j$, must be evaluated for each selected defect situation and for each cell size.

### Configurational entropy of oxygen-deficient perovskites with enthalpically preferred structural entities

Estimates of the configurational entropy of disordered materials where the number of vacancies per octahedron is restricted to one (square pyramids) or two (tetrahedra only) are derived. In both cases the defects are nearly randomly distributed at low defect concentrations. However, ordering is assumed to take place (due to defect–defect interactions) when a sufficiently large cluster of entities is formed; when the number of defect octahedra in a cell equals $a$. If we use as an example a disordered structure of $BO_6$ octahedra and $BO_5$ square pyramids, ordering takes place when the cell contains only $BO_5$ entities. In principle several different orientations of the local order may result. However, we assume that the lowest energy configuration is formed when the cell is "filled".

Under- and overestimates of the number of configurations and thus the configurational entropy are obtained by manual evaluation of the number of configurations of $j$ reduced entities of a given type in the ($y \times z$) cell. The size of the cells considered are (2 × 2) and (2 × 3) for square pyramids and (2 × 2) for tetrahedra. The underestimate is obtained by allowing only configurations that under no circumstances will give other entities than those considered. Hence, vacancies are not allowed at the surface-oxygen sites of the cells. The overestimate is obtained by allowing vacancies to form also here. Over- and underestimates of the configurational entropy of perovskites were only $BO_6$-octahedra and $BO_5$-square pyramids are present in the disordered state are given in Fig. 10a, whereas the

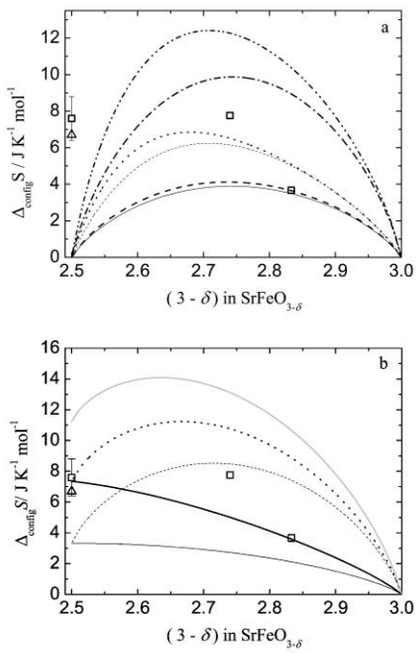


**Fig. 10** Comparison of configurational entropy assuming that one structural entity is preferred enthalpically with experimental determinations for $SrFeO_{2.500}$, $SrFeO_{2.740}$ and $SrFeO_{2.833}$. Squares – present study; triangle – ref. 37. Fig. 10a: square pyramids preferred, Fig. 10b: tetrahedra preferred. (a) Solid and short dashed lines, and dashed and dotted lines represent under- and overestimates for the (2 × 2) and (2 × 3) cells. Dashed dotted and dashed dot-dotted lines represent under- and overestimates for the (2 × 3) cell plus the entropy due to a random distribution of Fe(III) and Fe(IV) on the iron sub-lattice. (b) Thin and thick solid lines represent under- and overestimates for the (2 × 2) cell. Dotted and dashed lines represent over- and underestimates plus the entropy due to a random distribution of Fe(III) and Fe(IV) on the iron sub-lattice. The grey line represents the ideal entropy of Fig. 7.

entropy obtained if $BO_6$-octahedra and $BO_4$-tetrahedra are allowed is shown in Fig. 10b. The over- and underestimates of the configurational entropy together gives an interval for the configurational entropy that is comparable to the uncertainty of the calorimetric experiments when taking into consideration the assumptions for the electronic and vibrational contributions to the entropy of the structural order–disorder transitions and thus supports the presence of structural entities in the disordered materials at high temperatures.

The present structurally based description of the disordered state represents an alternative to defect-cluster models frequently used for dilute solutions. Exact mathematical approaches to the composition dependent site-exclusion factors needed for extending these models to high defect concentrations are not available.[38] Lattice energy simulations of the order–disorder transition in $SrFeO_{2.50}$ supports the presently proposed picture of the disordered state. The simulations suggests that the high-temperature phase can be described structurally as a mixture of octahedra, square pyramids and tetrahedra.[39]

## Conclusions

The excess heat capacity and the deduced entropy of $SrFeO_{3-\delta}$ is deconvoluted into vibrational, magnetic and structural

configurational contributions. The excess heat capacity of $SrFeO_{2.50}$ relative to the mixture of the binary constituent oxides is large even far below $T_N$ = 685 K due both to vibrational and magnetic effects. Lattice energy simulations show that the maximum in the excess heat capacity observed at around 60 K is due to a change in the vibrational density of state with origin in changes in the shortest Sr–O bond length on formation of the ternary oxide from the binary ones. While the entropy of the magnetic order–disorder transitions appears to be close to the ideal spin-only values, the entropy of the structural order–disorder transitions is much smaller than expected assuming random distribution of the relevant species on the different sub-lattices. A statistical analysis of the effect of enthalpically preferred structural entities (square pyramids or tetrahedra) on the configurational entropy is presented. A significantly reduced configurational entropy is obtained, in qualitative agreement with the experiments.

## References


1 K. Vidyasagar, A. Reller, J. Gopalakrishnan and C. N. R. Rao, *Chem. Commun.*, 1985, 7.
2 J. A. Alonso and M. J. Martinez-Lope, *Mater. Sci. Forum*, 1996, **228**, 747.
3 E. F. Bertaut, P. Blum and A. Sagnieres, *Acta Crystallogr.*, 1959, **12**, 149.
4 A. Colville, *Acta Crystallogr., Sect. B*, 1970, **26**, 1469.
5 V. Caignaert, N. Nguyen, M. Hervieu and B. Raveau, *Mater. Res. Bull.*, 1985, **20**, 479.
6 L. Er-Rakho, C. Michel and B. Raveau, *J. Solid State Chem.*, 1988, **73**, 514.
7 Y. Takeda, K. Kanno, T. Takada and O. Yamamoto, *J. Solid State Chem.*, 1986, **63**, 237.
8 C. Haavik, T. Atake, H. Kawaji and S. Stølen, *Phys. Chem. Chem. Phys.*, 2001, **3**, 3863.
9 S. Nakamura and S. Iida, *Jpn. J. Appl. Phys.*, 1995, **34**, L291.
10 K. Fournes, Y. Potin, J.C. Grenier, D. Demazeau and M. Pouchard, *Solid State Commun.*, 1987, **62**, 239.
11 J. P. Hodges, S. Short, J. D. Jorgensen, X. Xiong, B. Dabrowski, S. M. Mini and C. W. Kimball, *J. Solid State Chem.*, 2000, **151**, 190.
12 C. Haavik, DSc Dissertation, Faculty of Mathematics and Natural Sciences, University of Oslo, Norway, 2001.
13 J. C. Grenier, N. Ea, M. Pouchard and P. Hagenmuller, *J. Solid State Chem.*, 1985, **58**, 243.
14 J. B. MacChesney, R. C. Sherwood and J. F. Potter, *J. Chem. Phys.*, 1965, **43**, 1907.
15 H. Watanabe, *J. Phys. Soc. Jpn.*, 1957, **12**, 515.
16 T. C. Gibb, *J. Chem. Soc., Dalton Trans.*, 1985, 1455.
17 T. R. Clevenger, Jr., *J. Am. Ceram. Soc.*, 1963, **46**, 207.
18 T. Atake, H. Kawaji, A. Hamano and Y. Saito, *Rep. Res. Lab. Eng. Mater., Tokyo Inst. Technol.*, 1990, **15**, 13.
19 F. Grønvold, *Acta Chem. Scand.*, 1967, **21**, 1695.
20 S. Stølen, R. Glöckner and F. Grønvold, *J. Chem. Thermodyn.*, 1996, **28**, 1263.
21 S. Stølen and F. Grønvold, *Thermochim. Acta*, 1999, **327**, 1.
22 J. Gale, *J. Chem. Soc., Faraday Trans.*, 1997, **93**, 629.
23 B. G. Dick, Jr. and A. W. Overhauser, *Phys. Rev.*, 1958, **112**, 90.
24 O. H. Hansteen, Department of Chemistry, University of Oslo, personal communication.
25 C. Greaves, A. J. Jacobson, B. C. Tofield and B. E. F. Fender, *Acta Crystallogr. B*, 1975, **31**, 641.
26 J. C. Grenier, N. Ea, M. Pouchard and P. Hagenmuller, *J. Solid State Chem.*, 1985, **58**, 243.
27 S. Shin, M. Yonemura and H. Ikawa, *Mater. Res. Bull.*, 1978, **13**, 1017.
28 P. Adler, U. Schwarz, K. Syassen, A. P. Milner, M. P. Pasternak and M. Hanfland, *J. Solid State Chem.*, 2000, **155**, 381.
29 S. Stølen, *J. Chem. Thermodyn.*, 1998, **30**, 1495.
30 E. H. P. Cordfunke, R. R. van der Laan and J. C. van Miltenburg, *J. Phys. Chem. Solids*, 1994, **55**, 77.
31 F. Grønvold and E. J. Samuelsen, *J. Phys. Chem. Solids*, 1975, **36**, 249.
32 S. Stølen, F. Grønvold, H. Brinks, T. Atake and H. Mori, *J. Chem. Thermodyn.*, 1998, **30**, 365.
33 T. C. Gibb, *J. Mater. Chem.*, 1994, **4**, 1445.
34 M. Takano, T. Okita, N. Nakayama, Y. Bando, Y. Takeda, O. Yamamoto and J. B. Goodenough, *J. Solid State Chem.*, 1988, **73**, 140.
35 F. A. Kröger, F. H. Stieltjes and H. J. Vink, *Philips Res. Rep.*, 1959, **14**, 557.
36 J. A. M. Roosmalen and E. H. P. Cordfunke, *J. Solid State Chem.*, 1991, **93**, 212.
37 M. Schmidt and S. J. Campbell, *J. Solid State Chem.*, 2001, **156**, 292.
38 S. Diethelm, DSc Thesis No. 2436, Ecole Polytechnique Federale de Lausanne, Switzerland, 2001.
39 E. Bakken, N. L. Allan, H. Barron, C. Mohn, I. Todorov and S. Stølen, *Phys. Chem. Chem. Phys.*, submitted.